ISPRS Annals of the Photogrammetry, Remote Sensing and Spatial Information Sciences, Volume X-5/W2-2025
Unleashing the power of Geospatial & Frontier Technologies for a Sustainable Future – GIFTS Summit 2025,
1–3 September 2025, Symbiosis International University, Pune, India

Machine Learning Based Aircraft Detection using SAR & Optical Images

Madhura Rane[1, *], Shashi Kumar[2]
[1,2] Indian Institute of Remote Sensing, Indian Space Research Organization, Dehradun, India-
madhura.iirs@gmail.com,shashi@iirs.gov.in

Keywords: Aircraft Detection, SAR imagery, Optical imagery, Machine Learning, OCSVM, Isolation Forest.

Abstract

Aircraft detection in remote sensing imagery remains a critical challenge for surveillance and intelligence operations, with single-sensor approaches facing significant limitations that compromise operational effectiveness. This research addresses the integration of Synthetic Aperture Radar (SAR) and Optical imagery for enhanced aircraft detection through a novel computational framework. The study uses TanDEM-X SAR data (X-band, HH polarization) with up to 25 cm resolution in spotlight mode. Optical imagery is sourced from Google Earth Pro, providing high-resolution satellite data from platforms such as Landsat, Copernicus, and commercial providers. Computational models perform well even with small datasets, which is crucial when working with limited pre-paired SAR and optical data. This study proposes a three-phase computational framework that leverages complementary strengths of both sensors. The methodology encompasses aircraft template creation using edge detection and feature fusion, region detection via combined edge maps and SAR saliency, and multi-stage classification using One-Class SVM (OCSVM) and Isolation Forest algorithms. Feature-level fusion is implemented by extracting HOG, LBP, and statistical descriptors from optical imagery, and GLCM, texture, and intensity features from SAR data. The two-stage classification approach utilizes optical-based classification for geometric clarity, followed by SAR-optical fusion and Non-Maximum Suppression for improved reliability.
The framework achieved high aircraft detection accuracy, effectively handling challenges like limited data and cluttered backgrounds. This research contributes to the advancement of multi-sensor remote sensing applications by providing a practical, efficient solution for operational aircraft detection scenarios.

1. Introductions

Remote Sensing technologies are an integral part of modern surveillance and intelligence operations by offering reliable and continuous monitoring systems over extensive areas. Among them, radar-based imaging systems are ideal for strategic applications because of their all-weather and day-night working ability(Jitao Qin et al., 2019). The extraction of target texture and edge features plays a key role in the popularization and application of SAR(Karine et al., 2018). Over the years, various methods have been developed to improve aircraft detection in SAR images, each with its own strengths and limitations. Unlike traditional Constant False Alarm Rate (CFAR) algorithms that rely solely on statistical properties (Gagliardi & Reed, 1989), this framework integrates geometric, textural, and spectral information across multiple sensor modalities to achieve robust detection performance.

The sharp edges and metal surfaces of an aircraft's wings, body, and tail reflect radar signals intensely, creating strong backscatter. On SAR images, this backscattering creates bright spots in clustered patterns, which helps to distinguish aircraft from other objects. While SAR offers significant advantages, the process remains complex due to various challenges in the environments in which it operates. The task of aircraft identification becomes more complex due to similar objects within airports that share properties with aircraft(Tan et al., 2015).For example, objects like jetways have similar metallic structures, which may generate similar backscattering patterns, leading to potential misidentification.

In contrast, optical imagery offers high-resolution visual details that complement the strengths of SAR. Optical systems can provide fine-grained texture and color information that may not be visible in SAR images, especially in clear weather conditions. By combining both SAR and optical data, the accuracy of aircraft detection can be greatly improved, particularly in complex environments(Gao et al., 2022).

However, there are several key challenges in fusing SAR images to optical images for aircraft detection. One of the main obstacles is data scarcity; collecting aligned SAR and optical image pairs for aircraft is difficult due to differences in sensor characteristics and acquisition times. This lack of aligned datasets poses a challenge for training integrated models and achieving accurate fusion of the two types of imagery. This study is motivated by the increasing demand for precise and reliable aircraft identification solutions. As SAR technology continues to be a preferred option for tactical and defence operations, integrating optical data offers a way to address its existing limitations, improving detection accuracy, reducing false alarms, and enhancing the system's reliability, especially in difficult and unpredictable environments(Jitao Qin et al., 2019).

2. Methodology & Experiments

This section describes the overall methodology followed by its application to two experimental cases. Both experiments use the same processing pipeline, including template matching, saliency-based detection, feature extraction, and classification. The study area selected for this research is the Davis Monthan Air Force Base, located in Tucson, Arizona, United States (U.S. Air Force, 2024). The optical imagery component consists of high-resolution satellite data obtained from Google Earth Pro platform Fig1(b), providing access to various commercial satellite sources including Landsat, Copernicus, and high-resolution commercial providers.The SAR component utilizes TanDEM-X mission data from airbus Fig1(a).

This contribution has been peer-reviewed. The double-blind peer-review was conducted on the basis of the full paper.
https://doi.org/10.5194/isprs-annals-X-5-W2-2025-529-2025 | © Author(s) 2025. CC BY 4.0 License.

(a) *(b)*

Figure 1: (a) SAR image acquired from Airbus TanDEM-X mission (Spotlight mode) © Airbus DS 2025 (b) Optical image obtained from Google Earth Pro © Google Earth, Landsat/Copernicus, 2025.

The proposed methodology for aircraft detection using SAR and optical imagery integration follows a systematic multi-stage approach designed to leverage the complementary strengths of both sensor types. The framework(Fig.2) consists of three main phases: template generation, aircraft region detection, and machine learning classification.

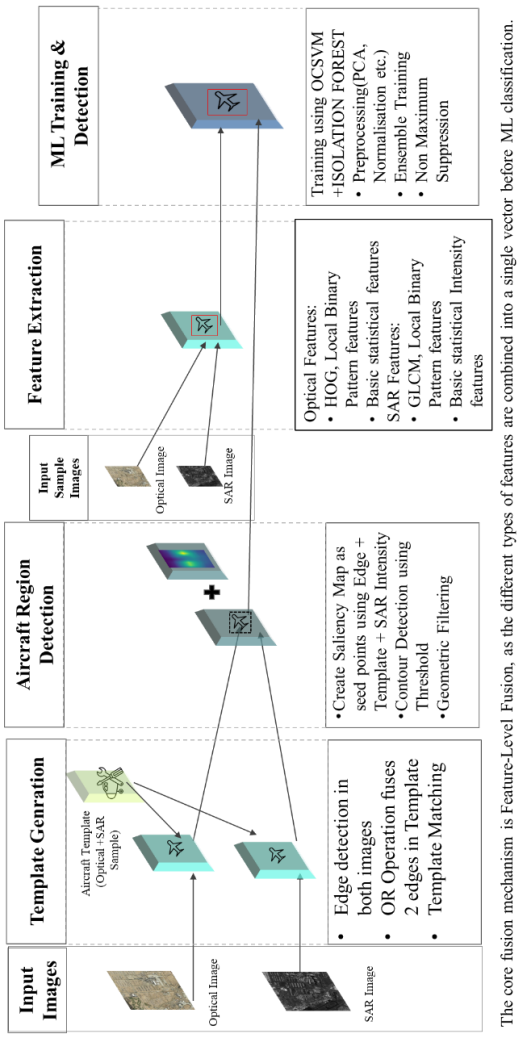

Figure 2: Conceptual Framework

The methodology, along with intermediate steps and classification processes, is depicted in Fig. 3.

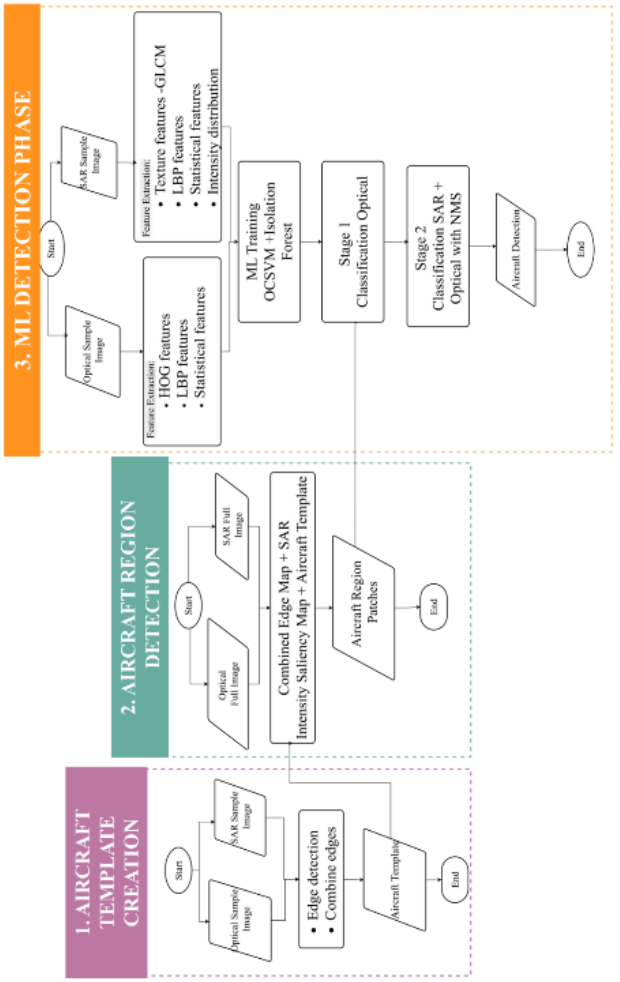

Figure 3: Methodology Optical+SAR

The below experiment was conducted on an 8m aircraft, as illustrated in the images(Fig.4).

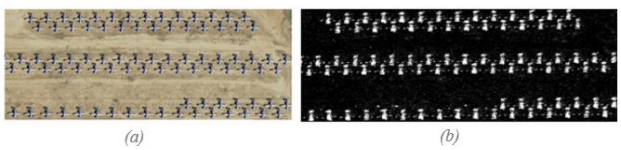

(a) *(b)*

Figure 4: 8m Aircrafts (a)Optical Image (b) SAR Image

The optical imagery preprocessing focused on shadow removal and geometric standardization to optimize feature extraction performance. Shadow removal was implemented using the Difference of Gaussians filter, which effectively eliminates shadow artifacts while preserving aircraft edge information(Fig.5 (b)). SAR data preprocessing was kept minimal to preserve radar signature integrity while ensuring geometric alignment with optical imagery. TanDEM-X SAR data was processed using SNAP to generate focused subsets, then resized to match the spatial resolution and extent of the optical data. Co-registration was performed using readily available referenced KML data to achieve accurate spatial alignment.

2.1 *Template Generation*

Aircraft template incorporates edge information from both SAR and optical imagery to create robust aircraft patterns for detection. The template generation process addresses aircraft

orientation variations through rotational analysis and combines complementary edge characteristics from both sensor types.
Edge detection forms the foundation of template generation, applied separately to SAR(Fig. 5(c)) and optical(Fig. 5(d)) imagery using optimized parameters for each sensor type.

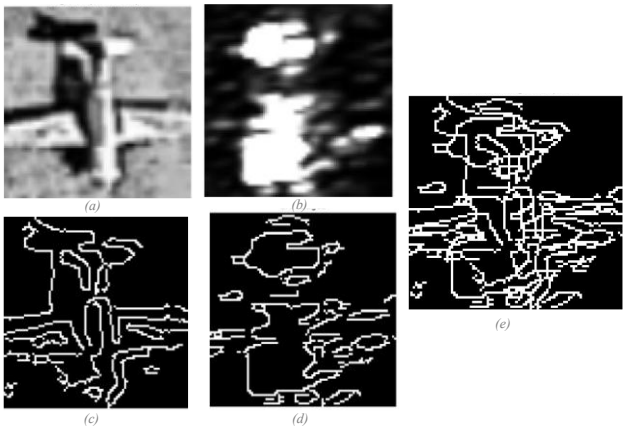

Figure 5: Template Generation Process Diagram (a)Optical Sample (b) SAR Sample (c) Optical Edge (d) SAR Edge (e) Combined Edge Template

The template fusion of SAR and optical edge information follows a logical OR operation to combine complementary edge information(Jitao Qin et al., 2019):

$$\text{Template} = \text{Optical\_edges OR SAR\_edges} \quad (1)$$

2.2 Aircraft Region Detection

Aircraft region detection uses the generated templates to identify potential aircraft locations within the study area through saliency mapping and contour analysis. Similar to template generation we use SAR edge(Fig.6 (c)) and optical edge(Fig.6 (e)) information using a logical OR operation to combine complementary edges(Fig.6 (f)). This stage also combines template matching(Fig.6(g)) with SAR intensity analysis(Fig.6(h)) to create comprehensive saliency maps highlighting probable aircraft regions(Fig.6 (i)).

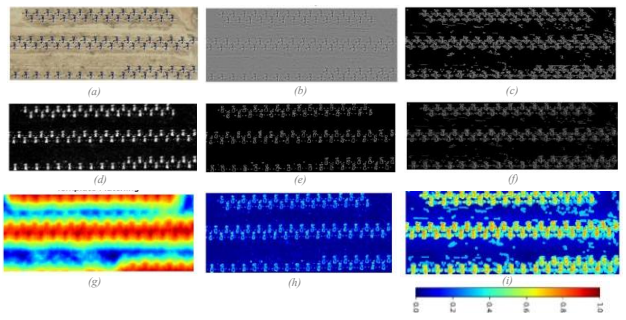

Figure 6: Saliency Map Generation Process (a) Optical Image (b) Optical Image after DOG (c) Optical Edge (d) SAR Image (e) SAR Edge (f) Combined Edge Image (g) Template Matching (h) SAR intensity (i) Combined Saliency

SAR intensity analysis helps detect potential aircraft by identifying bright regions in the image that are typical of metallic surfaces. Saliency maps are processed through four sequential steps to identify potential aircraft regions, as illustrated in Fig.7 (d, e & f). The process begins with binary thresholding (Fig.7(a)), which converts high-saliency areas into a binary mask, separating likely aircraft regions from the background based on confidence levels. Morphological processing (Fig.7 (b)) follows, using opening operations to remove small noise artifacts and close gaps within object boundaries, helping to form clean, continuous regions. Contour extraction (Fig.7 (c)) then detects the outlines of these regions using standard boundary detection techniques, providing accurate shape representations. Finally, geometric filtering is applied, enforcing constraints such as area limits and aspect ratio ranges that reflect realistic aircraft sizes and shapes, ensuring that only valid candidates proceed to the final detection stage.

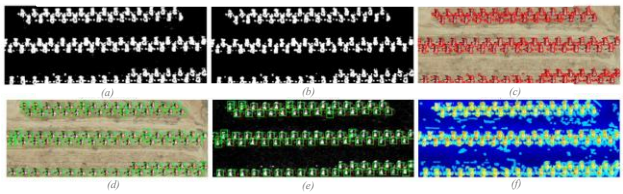

Figure 7: Contour Detection Results (a) Binary Threshold(0.4) (b) After Morphology Operations (c)All Contours (d) Optical Aircraft Region (e) Sar Aircraft Region (f)Saliency Aircraft Region

2.3 Feature Extraction

Feature extraction incorporates complementary information from both SAR and optical imagery to create comprehensive descriptors for aircraft classification. The feature extraction process combines geometric, textural, and statistical features optimized for multi-modal data characteristics.

2.3.1 Optical Image Features:

Histogram of Oriented Gradients (HOG) features are used to capture aircraft shape characteristics by analyzing the distribution of gradient orientations. The image is divided into cells of 8×8 pixels, with blocks formed by grouping 2×2 cells (16×16 pixels). Gradient orientations are binned into 9 bins spanning 0 to 180 degrees, and L2-norm normalization is applied within each block to ensure illumination invariance and robust feature extraction. The resulting HOG descriptor contains 3,780 features for a 128×64 pixel window, providing comprehensive shape representation.

Local Binary Pattern (LBP) features provide essential texture information that complements geometric HOG features(Tan et al., 2015). A radius of 3 pixels is used to define the local neighborhood for texture analysis, balancing detail capture with computational efficiency. To ensure thorough angular coverage, 24 sample points are uniformly distributed around each center pixel. The pattern type is set to uniform with rotation invariance, allowing the descriptor to remain robust under changes in aircraft orientation and lighting. Finally, the histogram is divided into 26 bins, representing 24 uniform patterns and 2 categories for non-uniform patterns, resulting in a compact yet expressive summary of local texture features.

Basic statistical measures provide additional discriminative information through two fundamental parameters. The mean intensity parameter calculates average pixel values within candidate regions, while the standard deviation parameter quantifies intensity variation. These statistical features complement geometric and texture descriptors by capturing regional brightness and surface heterogeneity characteristics that distinguish aircraft from background areas.

This contribution has been peer-reviewed. The double-blind peer-review was conducted on the basis of the full paper.
https://doi.org/10.5194/isprs-annals-X-5-W2-2025-529-2025 | © Author(s) 2025. CC BY 4.0 License.

2.3.2 SAR Image Features:

Gray-Level Co-occurrence Matrix (GLCM) analysis captures spatial texture relationships through five key parameters. The distance parameter examines immediate 1-pixel neighbours, while angles parameter covers four directions (0°, 45°, 90°, 135°) for comprehensive spatial analysis. Gray levels are quantized from 256 to 64 for computational efficiency. Five extracted features including contrast, dissimilarity, homogeneity, energy, and correlation provide robust texture descriptors that characterize aircraft surface patterns in SAR imagery.

GLCM features computed as(Zheng et al., n.d.):

$$Contrast = \Sigma\,\Sigma\,|i-j|^2 \times P(i,j) \quad (2)$$

$$Energy = \Sigma\,\Sigma\,P(i,j)^2 \quad (3)$$

$$Homogeneity = \Sigma\,\Sigma\,P(i,j) \,/\, (1 + |i-j|) \quad (4)$$

Where P(i,j) represents normalized co-occurrence matrix values.

In addition to texture and shape-based descriptors, backscattering(Jitao Qin et al., 2019) features derived from SAR imagery are also incorporated to enhance aircraft detection. These include the mean backscatter, which reflects the average σ^0 value within a region; the standard deviation and maximum backscatter, capturing intensity variations and peak responses; and histogram-based features that describe the distribution of intensity values. Advanced features such as edge density, intensity gradients, local contrast, and anisotropy are also included to capture spatial and directional properties of the backscatter signal. Together, these features form a comprehensive representation, resulting in a feature vector of approximately 12,000 dimensions, which is reduced to three principal components using PCA while retaining over 95% of the variance. All features undergo standardization to ensure equal contribution to classification

2.4 *Machine Learning Classification*

The classification framework uses a two-stage approach designed to optimize detection performance while minimizing false alarms. The first stage uses optical features for initial aircraft identification, followed by a second stage incorporating SAR features for refined classification and false positive reduction. The confusion matrix forms the foundational basis for evaluating classification performance in this study (Hastie et al., 2009). For binary classification (aircraft vs. non-aircraft), it comprises true positives (TP), false positives (FP), false negatives (FN), and true negatives (TN).

Precision, also known as Positive Predictive Value, is defined as

$$Precision = TP \,/\, (TP + FP) \quad (5)$$

This measures the proportion of predicted aircraft that are actually aircraft (Powers & Ailab, n.d.). It reflects the accuracy of positive predictions (Sokolova & Lapalme, 2009).

Recall, or Sensitivity/True Positive Rate, is calculated as

$$Recall = TP \,/\, (TP + FN) \quad (6)$$

It represents the proportion of actual aircraft correctly identified by the model (Bradley, 1997), indicating the completeness of positive predictions.

The F1-Score, defined as

$$F1 - Score = 2 \times (Precision \times Recall) \,/\, (Precision + Recall) \quad (7)$$

It provides the harmonic mean of precision and recall (Powers & Ailab, 2011) and is particularly important in aircraft detection tasks due to potential class imbalance.

Lastly, Accuracy is given by

$$\text{Accuracy} = (\text{TP} + \text{TN}) \,/\, (\text{TP} + \text{FP} + \text{FN} + \text{TN}) \quad (8)$$

It represents the overall proportion of correct predictions (Hastie et al., 2009). This metric remains widely used in remote sensing aircraft detection studies(Hameed & Khalaf, 2024).

2.4.1 Optical-Only Classification

One-Class Support Vector Machine (OCSVM) is the primary classifier for initial aircraft detection(Hameed & Khalaf, 2024; Jitao Qin et al., 2019), trained exclusively on positive aircraft samples. The algorithm is configured using a Radial Basis Function (RBF) kernel, with the gamma (γ) parameter automatically selected based on data distribution. An ensemble of One-Class SVM (OCSVM) models, each configured with varying parameter settings, is constructed to produce more reliable predictions by leveraging parameter variation. Feature input combines HOG, LBP, and statistical features for comprehensive aircraft characterization and detection performance(fig. 8). The missed detection (marked in red) in Fig.8 is due to its location at the image edge, which was excluded from the analysis.

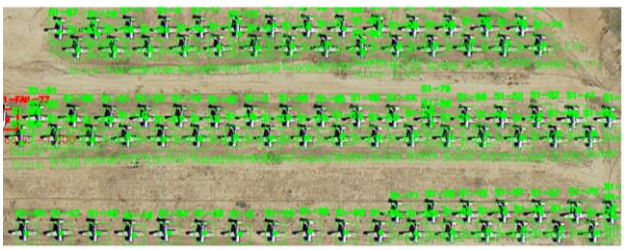

Figure 8: Stage 1 Classification Results Red: Failed Detection & Green: Passed Detections

The initial classification stage(Fig.8) utilized exclusively optical features extracted from high-resolution imagery to establish baseline detection capabilities for small aircraft targets. The performance evaluation was conducted on a test dataset comprising N=86 samples, yielding the confusion matrix presented in Table 3. The optical-only approach achieved a precision of 92.3% & perfect recall of 100%, resulting in an F1-score of 96% and overall accuracy of 93%. However, the precision of 92.3% reveals the presence of seven false positive detections, suggesting that there are multiple overlapping detections.

Actual\Predicted	TP	FP
TP	86	7
FN	0	1

Table 1: Confusion Metric Small Aircraft(8m) Stage-1

2.4.2 Combined SAR-Optical Classification

The second classification stage incorporates SAR features to refine detection results and recover missed aircraft from previous classification stage. Final classification combines OCSVM and Isolation Forest(Deepak et al., 2025) predictions through weighted score aggregation to leverage complementary detection strengths. Post-classification NMS eliminates duplicate detections through three sequential steps to ensure optimal detection selection(Fig. 9).

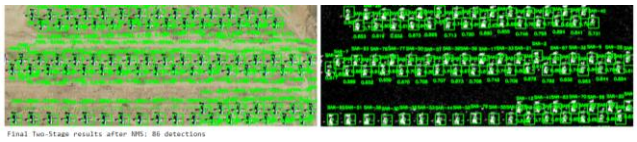

Figure 9: Stage 2 Classification Results (a)Optical Detection (b) SAR Detection(Green Aircraft Detected)

The integration of SAR data resulted in precision of 100% (86/86), recall of 100% (86/86), F1-score of 100%, and overall accuracy of 100% (86/86). Critically, all seven false positives from Stage 1 were correctly reclassified, demonstrating complete elimination of misdetections while maintaining perfect target detection capability(Table 2).

Actual\Predicted	TP	FP
TP	86	0
FN	0	8

Table 2: Confusion Metric Small Aircraft(8m) Stage-2

The complete elimination of false positives through NMS represents the resolution of spatial ambiguity that commonly occurs in sliding window detection approaches. The algorithm's ability to maintain perfect recall while achieving perfect precision indicates that the multi-modal feature space provides sufficient separability to establish optimal decision boundaries for true aircraft detection.

The second experiment applies the same workflow to a different scene(Fig.10), also involving an aircraft of similar size(12m) and characteristics. The corresponding inputs and detection results are shown in Figures 10 to 20. As the processing steps remain unchanged, only the results are presented here for comparison. This experiment provides a detailed analysis of how SAR data contributes to classification performance, particularly in situations where optical data alone is insufficient. It explores cases where SAR features offer critical information for distinguishing targets and quantifies the additional value SAR brings when combined with optical data.

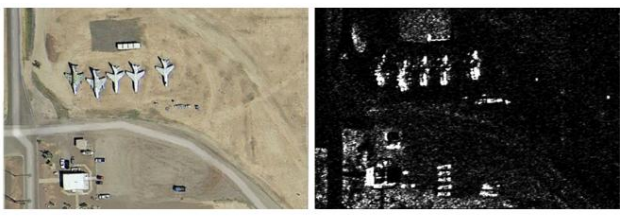

(a) (b)

Figure 10: 12m Aircrafts (a)Optical Image (b) SAR Image

The aircraft template generation process created robust templates incorporating edge information from both SAR and optical imagery(Fig.11).

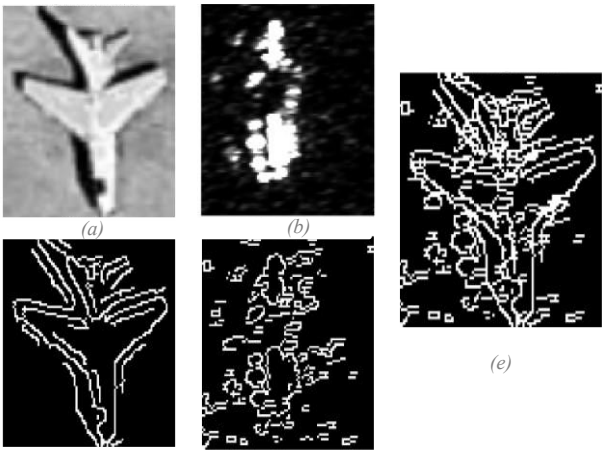

(a) (b) (c) (d) (e)

Figure 11: Template Generation Process Diagram (a)Optical Sample (b) SAR Sample (c) Optical Edge (d) SAR Edge (e) Combined Edge Template

The aircraft region detection phase identified candidate aircraft location. As mentioned earlier, the aircraft region detection phase employed integrated saliency mapping combined with morphological contour analysis to identify candidate target locations(Fig.12,13).

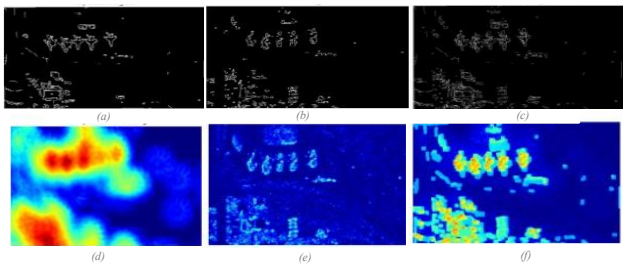

(a) (b) (c) (d) (e) (f)

Figure 12: Saliency Generation (a) Optical Edge (b) SAR Edge (c) Combined Edge Image (d) Template Matching (e) SAR intensity (f) Combined Saliency

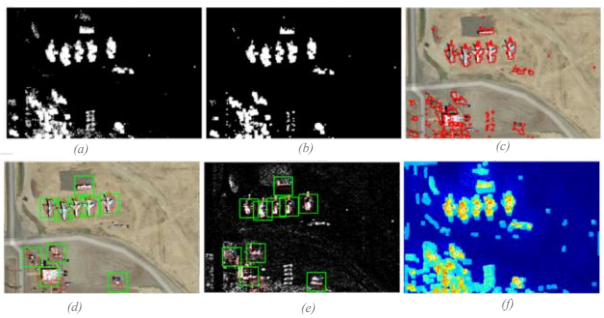

(a) (b) (c) (d) (e) (f)

Figure 13: Aircraft Region Detection (a) Binary Threshold(0.4) (b) After Morphology Operations (c)All Contours (d) Optical Aircraft Region (e) Sar Aircraft Region (f)Saliency Aircraft Region

The initial classification stage utilized HOG and LBP features extracted exclusively from optical imagery, evaluated on a test dataset comprising N=5 samples. The performance analysis revealed limitations in discriminative capability when relying solely on optical characteristics(Fig.14)& (Table 3). The optical-only approach achieved precision of 83.3% , perfect recall of 100%, F1-score of 91%, and overall accuracy of 90% . The presence of one false positive detection indicates fundamental limitations in the optical feature space's ability to distinguish

between aircraft targets and spectrally similar background objects, particularly building structures with comparable geometric characteristics.

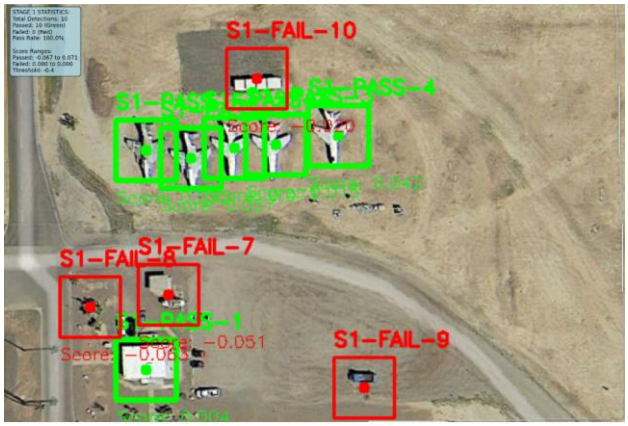

Figure 14: Stage 1 Classification Results Red: Failed Detection & Green: Passed Detections

Actual\Predicted	TP	FP
TP	5	1
FN	0	4

Table 3: Confusion Metric Small Aircraft(12m) Stage-1

The second classification stage incorporated SAR backscatter features alongside optical characteristics, implementing the established multi-modal fusion architecture(Fig.15). The integration of SAR data resulted in significant performance enhancement across all evaluation metrics(Table 4). In Stage 2, SAR fusion was applied to refine the detection results. While the optical-only features were effective in identifying 6 out of the 10 aircraft regions, Stage 2 demonstrated an improvement, as SAR fusion allowed for the correct classification of all 5 aircraft, eliminating the false positive from previous Stage.

Actual\Predicted	TP	FP
TP	5	0
FN	0	1

Table 4: Confusion Metric Small Aircraft(12m) Stage-2

The observed performance enhancement can be attributed to fundamental differences in electromagnetic scattering mechanisms between optical and microwave frequency domains. The results from Stage 1 indicate that optical features (HOG + LBP) were effective in detecting most aircraft but still had some limitations, producing 1 false positive. The false positive could have been caused by the difficulty of distinguishing the aircraft from the background. . In Stage 2, SAR fusion was applied to refine the detection process. The combination of SAR backscatter and optical features improved the classification accuracy, particularly by eliminating the false positive observed in Stage 1. In this stage, SAR data allowed for the correct classification of all 5 aircraft, ensuring 100% detection accuracy.

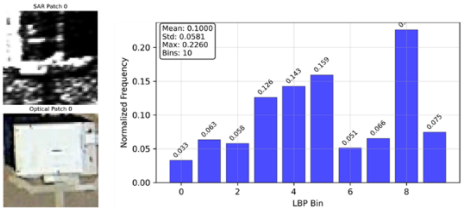

Figure 15: LBP Building Features

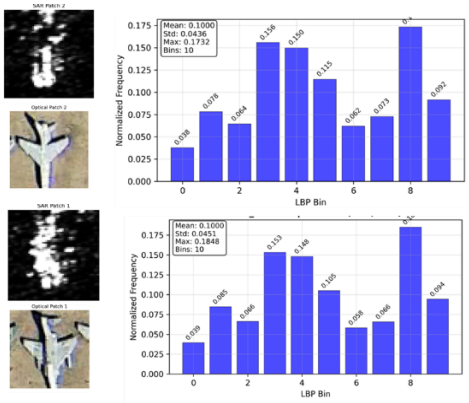

Figure 16: LBP Aircraft Features

LBP analysis reveals distinct textural patterns, with buildings showing ascending values in bins 3–5 due to complex surface variations, while aircraft exhibit a descending trend reflecting smoother materials.

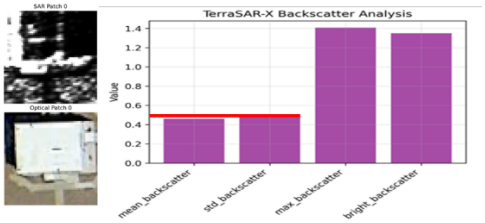

Figure 17: Backscattering Building Features

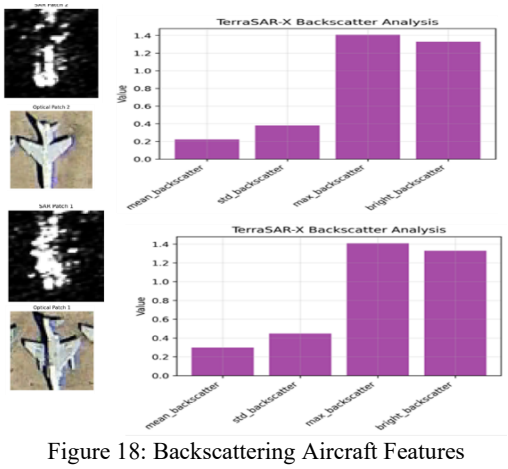

Figure 18: Backscattering Aircraft Features

SAR backscatter analysis reveals that buildings produce higher mean backscatter due to distributed scattering from rough construction materials, while aircraft exhibit lower intensities owing to specular reflections from smooth, metallic surfaces. This contrast offers complementary discrimination based on surface and material properties.

This contribution has been peer-reviewed. The double-blind peer-review was conducted on the basis of the full paper.
https://doi.org/10.5194/isprs-annals-X-5-W2-2025-529-2025 | © Author(s) 2025. CC BY 4.0 License.

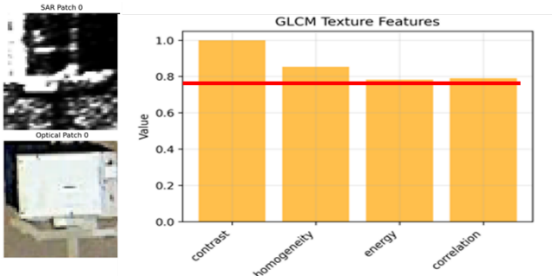

Figure 19: GLCM Building Features

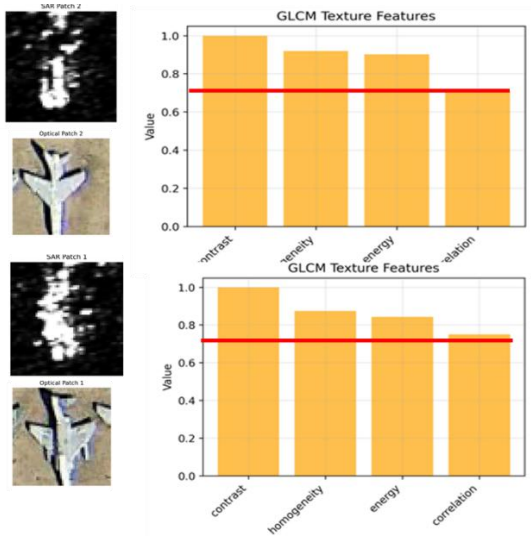

Figure 20: GLCM Aircraft Features

GLCM energy analysis highlights textural differences, with buildings showing low energy values <0.8 to high surface variation, while aircraft exhibit high values >0.8 reflecting uniform, smooth surfaces.

Compared with the SAR–optical fusion approach of (Jitao Qin et al., 2019), which achieved a precision of 75.56% with a 20% false alarm rate, our adapted method attained 100% precision with no false alarms on the test dataset. While this is a substantial improvement over both their HIS fusion method (21.43% precision) and optical-only method (66.67% precision), these results should be viewed as preliminary, given the limited dataset and controlled acquisition conditions.This analysis conclusively demonstrates that SAR features provide essential enhancement to aircraft detection accuracy by enabling precise discrimination between aircraft (high metallic backscatter) and building structures (low non-metallic backscatter), even when optical features show similarity between these object type.

3. Conclusion

The experimental findings show that the suggested SAR-optical fusion framework performs noticeably better than single-sensor methods, attaining high aircraft detection accuracy while maintaining computational viability. In complex situations, the two-stage classification system improves detection reliability, particularly when SAR is integrated into Stage 2. Because there aren't many positive training samples for the aircraft detection problem, the algorithms chosen are especially well-suited.
Its operational robustness and generalizability must be fully established through additional validation in more intricate and cluttered environments.

4. Acknowledgments

The authors gratefully acknowledge Airbus Defence and Space for providing sample synthetic aperture radar (SAR) imagery from the TanDEM-X mission, accessed via the Airbus Space Solutions portal. The optical imagery was obtained from Google Earth Pro and contains Landsat/Copernicus data courtesy of the United States Geological Survey (USGS), the National Aeronautics and Space Administration (NASA), and the European Space Agency (ESA). All data processing, analysis, and visualization were carried out using the Jupyter interactive computing environment.

5. References

B, A. P. (2019). *The Use of the Area Under the ROC Curve in the Evaluation of Machine Learning Algorithms Draft Only 2*.

Deepak, D., Gowtham, P. P. V, Vali, S. B., & Meenu Teja, T. (2025). Intelligent AI and Iot System for Object Detection and Missile Launching in Military Applications. In *International Journal of Enhanced Research in Science* (Vol. 14).

Distribution, N. (1989). *Final Technical Report ADAPTIVE MULTIPLE-BAND CFAR i rDETECTION OF AN OPTICAL SPATTERN WITH UNKNOWN*.

Gao, Q., Feng, Z., Yang, S., Chang, Z., & Wang, R. (2022). Multi-Path Interactive Network for Aircraft Identification with Optical and SAR Images. *Remote Sensing*, *14*(16). https://doi.org/10.3390/rs14163922

Hameed, M. A., & Khalaf, Z. A. (2024). An Approach for Aircraft Detection using VGG19 and OCSVM. *International Journal of Computing and Digital Systems*, *16*(1), 115–124. https://doi.org/10.12785/ijcds/160109

Hastie, T., Tibshirani, R., & Friedman, J. (2009). *The Elements of Statistical Learning: Data Mining, Inference, and Prediction, Second Edition (Springer Series in Statistics)*.

Jitao Qin, Haicheng Qu, Hao Chen, & Wen Chen. (2019). *2019 IEEE International Geoscience & Remote Sensing Symposium : proceedings : July 28-August 2, 2019, Yokohama, Japan*. IEEE.

Karine, A., Toumi, A., Khenchaf, A., & El Hassouni, M. (2018). Radar target recognition using salient keypoint descriptors and multitask sparse representation. *Remote Sensing*, *10*(6). https://doi.org/10.3390/rs10060843

Powers, D. M. W., & Ailab. (n.d.). *EVALUATION: FROM PRECISION, RECALL AND F-MEASURE TO ROC, INFORMEDNESS, MARKEDNESS & CORRELATION*.

Sokolova, M., & Lapalme, G. (2009). A systematic analysis of performance measures for classification tasks. *Information Processing & Management*, *45*, 427–437. https://doi.org/10.1016/j.ipm.2009.03.002

Tan, Y., Li, Q., Li, Y., & Tian, J. (2015). Aircraft detection in high-resolution SAR images based on a gradient textural saliency map. *Sensors (Switzerland)*, *15*(9), 23071–23094. https://doi.org/10.3390/s150923071

Zheng, Z., Jixian, Z., Guoman, H., & Wang, R.-. (n.d.). *THE TEXTURAL ANALYSIS AND INTERPRETATION OF HIGH RESOLUTION AIRSAR IMAGES*.

Airbus. (2025). *Radar Constellation: Tucson, AZ, USA – Spotlight imagery*. Airbus Space Solutions. Available at: https://space-solutions.airbus.com/imagery/sample-imagery/radar-constellation-tucson-az-usa-staring-spot-light/ (Accessed: 4 July 2025).

Google Earth Pro. (2025). *Landsat imagery of Tucson, Arizona, USA*. Available at: https://earth.google.com/ (Accessed: 4 July 2025).